Midbrain dopaminergic innervation of the hippocampus is sufficient to modulate formation of aversive memories

Theodoros Tsetsenis[a,1], Julia K. Badyna[a], Julianne A. Wilson[b], Xiaowen Zhang[b], Elizabeth N. Krizman[b,c], Manivannan Subramaniyan[a], Kechun Yang[a], Steven A. Thomas[b,2], and John A. Dani[a,1,2]

[a]Department of Neuroscience, Mahoney Institute for Neurosciences, Perelman School for Medicine, University of Pennsylvania, Philadelphia, PA 19104; [b]Department of Systems Pharmacology and Translational Therapeutics, Perelman School for Medicine, University of Pennsylvania, Philadelphia, PA 19104; and [c]Department of Pediatrics, Children's Hospital of Philadelphia, University of Pennsylvania, Philadelphia, PA 19104

Edited by Peter L. Strick, University of Pittsburgh, Pittsburgh, PA, and approved August 9, 2021 (received for review June 19, 2021)

Aversive memories are important for survival, and dopaminergic signaling in the hippocampus has been implicated in aversive learning. However, the source and mode of action of hippocampal dopamine remain controversial. Here, we utilize anterograde and retrograde viral tracing methods to label midbrain dopaminergic projections to the dorsal hippocampus. We identify a population of midbrain dopaminergic neurons near the border of the substantia nigra pars compacta and the lateral ventral tegmental area that sends direct projections to the dorsal hippocampus. Using optogenetic manipulations and mutant mice to control dopamine transmission in the hippocampus, we show that midbrain dopamine potently modulates aversive memory formation during encoding of contextual fear. Moreover, we demonstrate that dopaminergic transmission in the dorsal CA1 is required for the acquisition of contextual fear memories, and that this acquisition is sustained in the absence of catecholamine release from noradrenergic terminals. Our findings identify a cluster of midbrain dopamine neurons that innervate the hippocampus and show that the midbrain dopamine neuromodulation in the dorsal hippocampus is sufficient to maintain aversive memory formation.

fear conditioning | optogenetics | ventral tegmental area | substantia nigra pars compacta | locus coeruleus

Dopaminergic signaling regulates a diverse array of behaviors in the mammalian central nervous system (1). In addition to its well-established role in the control of movement (2, 3), motivation (4, 5), and reward processing (6, 7), dopamine (DA) also modulates hippocampus-dependent learning and memory (8–10). This heterogeneity of effects depends strongly on the target as well as the origin of the dopaminergic signal. Recent studies indicate that certain subpopulations of midbrain DA neurons located in the ventral tegmental area (VTA) and substantia nigra pars compacta (SNc) send projections to specific target areas in the ventral and dorsal striatum, amygdala, prefrontal cortex, and other forebrain structures (11, 12). Surprisingly, very limited information exists about midbrain dopaminergic projections to the hippocampus.

Studies from the 1990s in the rat suggested that dopaminergic projections from the midbrain (VTA, SNc, and retrorubral field) are the main source of hippocampal DA (13–15). Those observations found support in more recent studies showing that these projections can modulate synaptic responses in hippocampal CA1 (16), regulate drug-induced in vivo synaptic plasticity (17), and facilitate spatial memory retention (18). Nevertheless, the discrepancy between the low density of dopaminergic fibers and the high expression of D1/D5 receptors (19–21) suggested the existence of other sources of DA in the rodent hippocampus (22, 23). In fact, it was shown that the optogenetic activation of tyrosine hydroxylase (TH)–positive neurons in the locus coeruleus (LC) also enhances spatial memory (24, 25). Those neurons synthesize DA as a precursor of norepinephrine (NE), and they corelease both neurotransmitters in the hippocampus, acting as an alternative source of DA (22, 24, 25). The higher density of TH innervation from the LC has led to the expectation that DA from the midbrain may be relatively insignificant. Strikingly, however, both midbrain dopaminergic and LC projections to the dorsal hippocampus (dHip) can promote the consolidation of spatial memory in different tasks (18, 24). Furthermore, NE itself has been shown to play an important role in hippocampus-dependent memory processes (26, 27). Thus, there are considerable complications surrounding the source and function of hippocampal DA in different mnemonic processes.

In addition to its role in the regulation of spatial memory retention, DA has been strongly associated with the formation of aversive memories. It is known that aversive stimuli (28, 29), as well as threat-predictive cues (30, 31), can trigger the firing of a subpopulation of midbrain dopaminergic neurons and elevate DA levels in the forebrain (32–34). In the hippocampus, it has been shown that dopaminergic transmission is necessary for aversive learning and associated synaptic plasticity, and inhibition of D1/D5 receptors in the dorsal CA1 (dCA1) impairs performance in a passive avoidance task (10, 35). Even though there is considerable evidence supporting the notion that the inhibition of hippocampal DA signaling impairs aversive learning, the source of the DA signals

Significance

The origin and mode of action of dopamine on hippocampus-dependent memory have been a matter of interest for many years. The latest research has pointed toward the locus coeruleus as the main source of hippocampal dopamine, while inputs from midbrain dopaminergic centers remain controversial and understudied. We provide anatomical evidence for a direct dopaminergic projection to the hippocampus from a distinct, identified midbrain population and report a bidirectional modulation of hippocampal-aversive learning by midbrain dopamine. Our data indicate that this modulation is sustained even in the absence of catecholamine release from the locus coeruleus. These results demonstrate that midbrain dopaminergic innervation of the dorsal hippocampus is significant and plays a functional role in the modulation of aversive memory formation.

Author contributions: T.T., S.A.T., and J.A.D. designed research; T.T., J.K.B., J.A.W., X.Z., E.N.K., M.S., K.Y., and S.A.T. performed research; T.T., J.K.B., E.N.K., K.Y., and S.A.T. analyzed data; and T.T. and J.A.D. wrote the paper.

The authors declare no competing interest.

This article is a PNAS Direct Submission.

[1]To whom correspondence may be addressed. Email: theot@pennmedicine.upenn.edu or johndani@pennmedicine.upenn.edu.

[2]S.A.T. and J.A.D. contributed equally to this work.

This article contains supporting information online at https://www.pnas.org/lookup/suppl/doi:10.1073/pnas.2111069118/-/DCSupplemental.

Published September 27, 2021.

and the way DA contributes to this process remain understudied and unresolved.

In this study, we used complementary retrograde and anterograde tracing techniques to show the dopaminergic innervation of dCA1 and to identify a population of dopaminergic neurons in VTA/SNc that projects directly to the hippocampus. Next, we utilized contextual fear conditioning (cFC) as a paradigm to test the effects of midbrain dopaminergic transmission on aversive memory formation in the hippocampus. Using optogenetics to enhance midbrain DA transmission and pharmacology to inhibit DA signaling in dCA1, we found that DA can bidirectionally regulate context-dependent, associative fear learning. Finally, by genetic ablation of catecholamine production exclusively in NE neurons, we showed that midbrain DA (with no LC DA contribution) is sufficient to maintain normal contextual fear memory formation.

Results

A Population of Dopaminergic Neurons Located in the SNc and Lateral VTA Directly Projects to the Dorsal Hippocampus. To date, there has not been a comprehensive study investigating dopaminergic innervation of the mouse hippocampus, and recent efforts using advanced technologies to map inputs and outputs of the midbrain DA areas have not examined the hippocampus (11). In our efforts to address this problem, we used an anterograde, viral tracing methodology to examine the existence of a direct midbrain dopaminergic projection to the dHip (Fig. 1*A*) (10, 36). This method utilizes an adeno-associated virus (AAV) expressing synaptophysin fused with a fluorescent protein (mRuby) exclusively in midbrain dopaminergic neurons of the VTA/SNc (Fig. 1*B*). The localization of synaptophysin fusion proteins in synaptic vesicles results in an enriched fluorescent signal in DA neuronal terminals, because there are multiple synaptophysin molecules per vesicle and multiple vesicles per terminal. In the dorsal hippocampal CA1 region (Fig. 1*C*), in particular, we observed the punctate staining of fluorescence-labeled terminals along the pyramidal cell layer (PCL), as well as a few sparse fiber tracts in stratum oriens (SO) and stratum radiatum (SR) (Fig. 1*D*). These labeled puncta were also positive for TH (94.6 ± 2.0% and $n = 5$ mice), further confirming their midbrain dopaminergic origin (Fig. 1 *E* and *F*).

To reliably identify and label the midbrain populations that directly project to the dHip, we used a combination of retrograde, viral approaches. First, we injected canine adenovirus type 2 expressing Cre recombinase (CAV2-Cre) (37) into the dHip of Ai14 Cre-dependent tdTomato reporter mice (38) to label selectively neurons that send axons to this area (Fig. 2 *A* and *B*). Histological analysis confirmed direct inputs to the dHip from several brain regions, including a population of neurons in the anterior midbrain area. When counterstained with an antibody against TH, we found that tdTomato-positive cells located in the interface between the lateral VTA and SNc coexpressed TH,

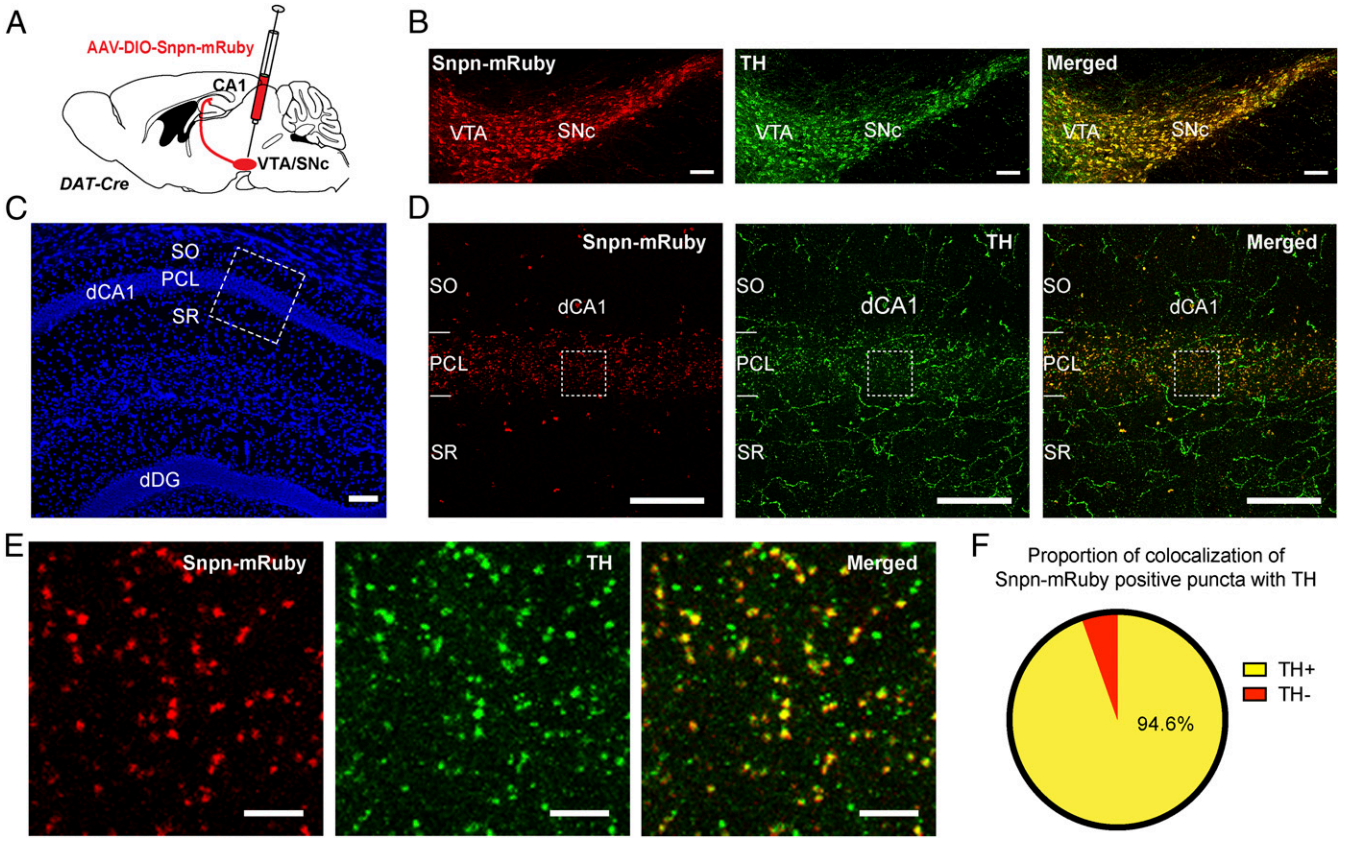

Fig. 1. Anterograde tracing of VTA/SNc dopaminergic projections to the CA1 hippocampal field. (*A*) An AAV allowing the conditional expression of a synaptophysin-mRuby fusion protein (AAV-DIO-Snpn-mRuby) was injected into the VTA/SNc of DAT-Cre mice to facilitate anterograde labeling of DA terminals originating from the midbrain. (*B*) Coronal midbrain section showing the infection in the VTA/SNc with Snpn-mRuby (red, *Left*), labeling of DA cells with TH (green, *Middle*), and a merged image showing the colocalization of Snpn-mRuby–infected cells with TH (orange/yellow, *Right*). (Scale bars, 100 μm.) (*C*) Representative low-magnification coronal section of dCA1 stained with DAPI. The boxed area corresponds to the high-magnification images of dCA1 in *D*. (Scale bar, 100 μm.) (*D*) Coronal section of dCA1, corresponding to the boxed area in *C* showing DA terminals expressing Snpn-mRuby (red, *Left*) immunostained with an antibody against TH (green, *Middle*) and a merged image showing the colocalization of the two markers. (Scale bars, 50 μm.) (*E*) Higher-magnification images of the boxed areas in *D*, showing that anterogradely labeled terminals coexpress TH (yellow, *Right*). (Scale bars, 5 μm.) (*F*) Percentage of Snpn-mRuby–positive puncta that are also positive for TH (Snpn-mRuby/TH double-positive: 94.6 ± 2.0% and $n = 5$ mice). Data represent means ± SEM. dDG, dorsal dentate gyrus.

verifying their dopaminergic identity (Fig. 2 *C* and *D*). The distribution of tdTomato/TH double-positive neurons was more prominent in the anterior part of the SNc, with fewer cells in the posterior part and approximately half of the tdTomato-labeled cells in the VTA/SNc being dopaminergic (*SI Appendix*, Fig. S1*A*). The histological examination of the CAV-Cre injection area showed no signs of viral spread in the neighboring striatum tail, a region that receives strong midbrain dopaminergic innervation, eliminating the probability of an off-target labeling effect (*SI Appendix*, Fig. S1*C*). To also exclude the possibility that retrograde labeling of these midbrain cells was a result of CAV2-Cre leakage along the injection path above the hippocampus, we performed control injections in which we confined the viral spread to the cortical layers directly above the dHip (*SI Appendix*, Fig. S1*D*). In contrast to what we observed with our injections into the hippocampus, no labeled cells were present in the midbrain of Ai14 mice when CAV2-Cre was targeted in these superficial cortical areas just above the dHip, ruling out a possible artifact due to off-target viral spread.

To verify our finding and to characterize these dopaminergic neurons further, we utilized a second approach that allows the direct labeling of DA neurons that project to the hippocampus (Fig. 2*E*). Specifically, we injected a retrograde canine adenovirus expressing a Cre-dependent Flp recombinase (CAV-FLEX-Flp) into the dHip of DAT-IRES-Cre$^{\pm}$ (DAT-Cre) mice followed by the injection of AAV expressing a Flp-dependent version of eYFP (AAV-fDIO-eYFP) into the VTA/SNc. This procedure resulted in the expression of eYFP, specifically, in midbrain DA neurons projecting to the hippocampus (Fig. 2*F* and *SI Appendix*, Fig. S1*B*). Consistent with our first approach, a population of neurons in the lateral VTA and adjacent SNc expressed eYFP. These cells exhibited electrophysiological properties typical of

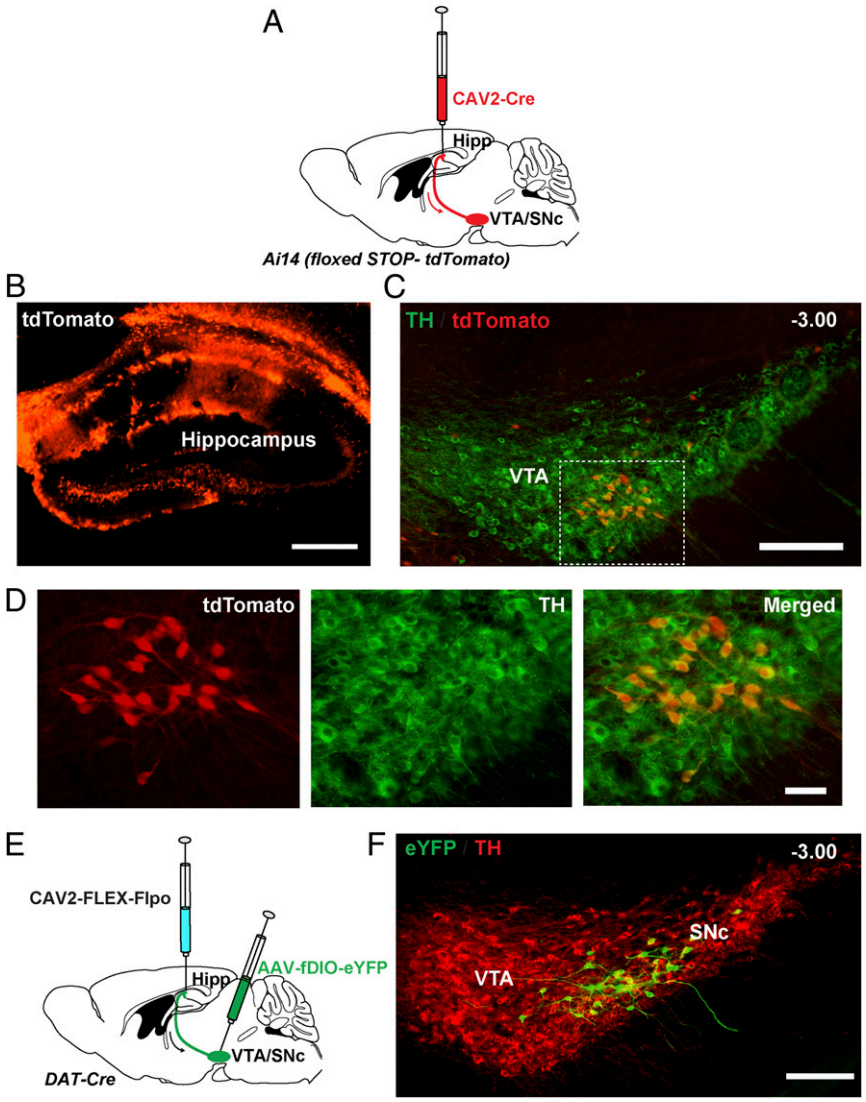

Fig. 2. Retrograde tracing identifies a population of DA neurons in the anterolateral VTA/SNc that directly projects to the hippocampus. (*A*) CAV2-Cre injected into the hippocampus of Ai14 reporter mice to allow the retrograde labeling of projection neurons. (*B*) Coronal section showing the infection of the dHip of Ai14 mouse with CAV-Cre and the induction of tdTomato expression in infected cells. (Scale bar, 100 μm.) (*C*) Coronal section of anterolateral VTA/SNc showing retrogradely labeled neurons expressing tdTomato (red) and immunostained with an antibody against TH (green). (Scale bar, 200 μm.) (*D*) Higher magnification of the boxed area in *C*, showing that retrogradely labeled cells coexpress TH. (Scale bar, 50 μm.) (*E*) CAV2-Flex-Flpo was injected in the dHip of DAT-Cre mice, and AAV-DIO-eYFP was injected in the anterior VTA/SNc. (*F*) Coronal section of anterolateral VTA/SNc showing retrogradely labeled DA neurons expressing YFP (green) and immunostained with an antibody against TH (red) to highlight the VTA/SNc region. As before in *C* and *D*, labeled neurons are located in the SNc and lateral VTA. (Scale bar, 200 μm.) The numbers on the top right corner represent the distance from bregma (65).

dopaminergic neurons. The resting membrane potential and input resistance (*SI Appendix*, Fig. S2*A*), as well as firing frequency (*SI Appendix*, Fig. S2*B*) and hyperpolarization-activated (I_h) current amplitude (*SI Appendix*, Fig. S2*C*), were similar to unlabeled dopaminergic neurons in the same area. We did not observe any YFP-positive fibers in the dorsal and ventral striatum, prefrontal cortex, or amygdala, suggesting that these hippocampal-projecting neurons do not send extensive collateral projections to these areas. These results demonstrate that there is a direct dopaminergic innervation of the dHip from an identified cluster of dopaminergic neurons in the anterior VTA/SNc.

Optogenetic Activation of Midbrain Dopaminergic Terminals in dCA1 Enhances Contextual Fear Memory. cFC is a hippocampus-dependent, associative learning process that can be used to assess aversive memory in rodents and humans (39). Since midbrain dopaminergic centers send projections to the dCA1, we next wanted to examine the effects of increased DA transmission in this region on cFC encoding. To control the activity of midbrain dopaminergic neurons, we injected a Cre-dependent AAV encoding channelrhodopsin-2 fused to an enhanced yellow fluorescent protein (ChR2-eYFP) into the lateral VTA/SNc of DAT-Cre mice (Fig. 3*A*). This mouse line has been repeatedly shown to enable the targeting of midbrain

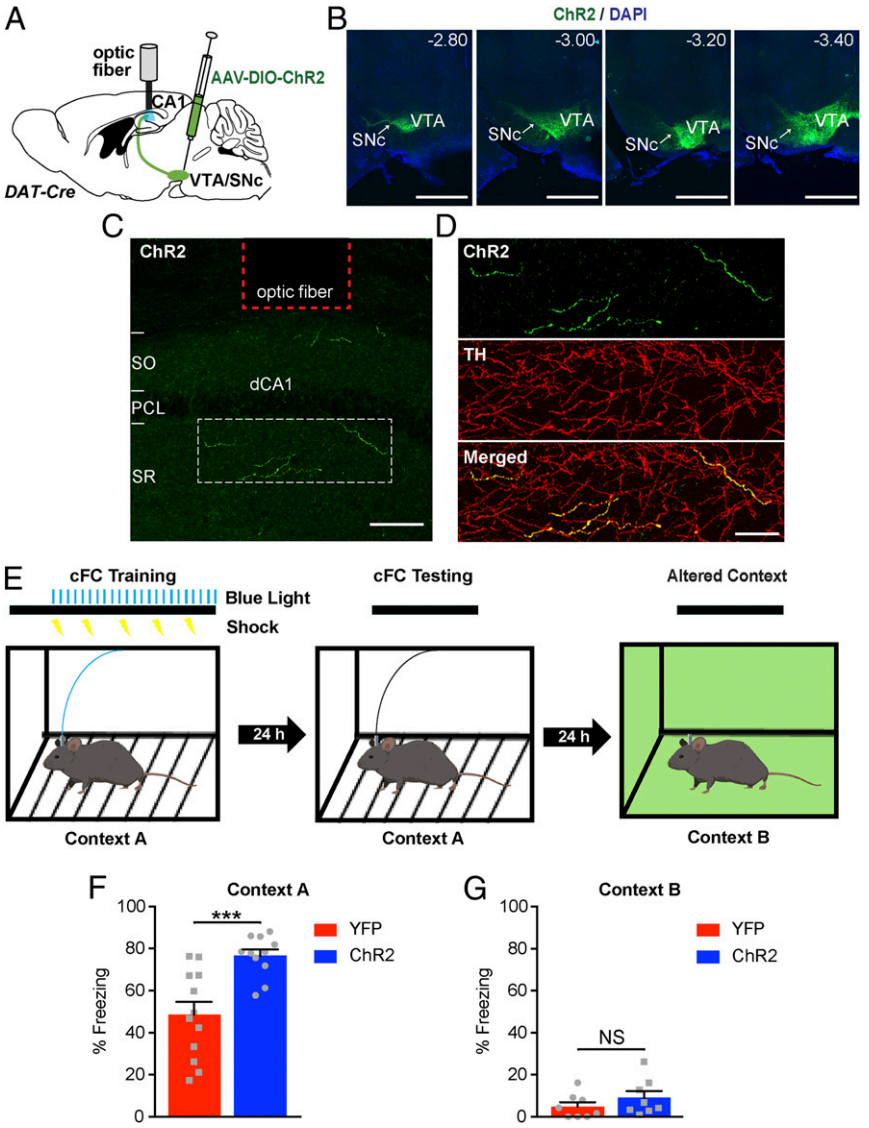

Fig. 3. Optogenetic activation of midbrain dopaminergic terminals in dCA1 during cFC training causes an increase in freezing responses during recall in a context-specific manner. (*A*) An AAV encoding Cre-dependent ChR2-eYFP was bilaterally injected in the VTA/SNc of DAT-Cre mice, and optic fibers were implanted above the dCA1. (*B*) Coronal sections from the midbrain of a DAT-Cre mouse injected with AAV-DIO-ChR2-eYFP were immunostained with an antibody against GFP to enhance eYFP fluorescence to visualize ChR2 expression and DAPI. The numbers on the top left corner represent the distance from bregma (65). (Scale bar, 1 mm.) (*C*) Confocal image of the dCA1 from the same mouse as in *B* showing the expression of ChR2-positive fibers and optic fiber placement. (Scale bar, 100 μm.) (*D*) High magnification of dashed box in *C* showing the colocalization of ChR2-positive fibers with TH. (Scale bar, 50 μm.) (*E*) Schematic illustration of cFC procedure. A horizontal black line with light trains as vertical blue bars and shocks as lightning bolts represents the timeline of the exposure to each context. Blue light delivery and shocking occurred only during training. (*F*) Bar graph showing the freezing responses of ChR2-positive and YFP control mice after reexposure to context "A" 24 h after training. Unpaired Student's *t* test, $P = 0.0007$; $n = 12$ and 11 for YFP and ChR2, respectively; $^{***}P < 0.001$; and data represent means ± SEM. (*G*) Graph showing freezing responses of ChR2-positive and YFP control mice in an altered context "B" 24 h after reexposure to context A. Unpaired Student's *t* test, $P = 0.270$; $n = 8$ for YFP and ChR2; not significant (NS): $P > 0.05$; and data represent means ± SEM.

dopaminergic neurons with high specificity, >95% of Cre+ neurons coexpress TH (40). In these mice ($ChR2^{VTA/SNc}$), we found the widespread expression of ChR2-eYFP in dopaminergic neurons spanning from anterior to posterior VTA and SNc (Fig. 3*B*). Then, we examined the projections of these $ChR2^{VTA/SNc}$ dopaminergic neurons. In addition to their presence in areas such as the striatum, amygdala, and PFC, axons coexpressing ChR2-eYFP and TH were also found in the dCA1 region of the hippocampus (Fig. 3 *C* and *D*, green fiber tracks). These data are consistent with previous studies (10, 16, 18, 25) showing the sparse but significant innervation of dCA1 by dopaminergic neurons.

In these mice, we implanted optic fiber cannulas above the dCA1 (*SI Appendix*, Fig. S3) in order to stimulate the release from dopaminergic terminals evoked by blue-light delivery. To evaluate the effects of increased dopaminergic transmission in dCA1 on the acquisition of aversive memory, we trained fiber-implanted $ChR2^{VTA/SNc}$ mice and $YFP^{VTA/SNc}$ (i.e., control) mice using a modified cFC protocol (Fig. 3*E*). After a 2-min exploration period, mice received a series of five foot shocks (0.4 mA, 1 s, with pseudorandomized intervals averaging 2 min), while also receiving pulses of blue light (450 nm, 10 ms at 20 Hz for 1 s every 10 s) that started together with the first foot shock and continued until the end of the training session. The next day, the mice were returned to the same chamber, and their fear memory was assessed without optical stimulation or foot shocks by calculating the time spent freezing. Strikingly, the optogenetic increase of dopaminergic transmission in the dCA1 of ChR2-positive mice during cFC training resulted in significantly higher freezing responses than those of control mice (Fig. 3*F* and Movie S1). Significantly, larger freezing responses of $ChR2^{VTA/SNc}$ mice persisted during the subsequent days of testing but gradually decreased in strength down to control levels by the fourth day of testing (*SI Appendix*, Fig. S4 *A* and *B*). Interestingly, no differences in freezing were observed when the optogenetic stimulation of DA release was not coupled with shock delivery but, rather, was done 5 min after the end of cFC training (*SI Appendix*, Fig. S4 *C* and *D*). These results indicate that DA from the VTA/SNc released in the dCA1 during the acquisition of fear memory enhances the association between contextual cues and the aversive experience.

To exclude the possibility that the effect we observed was due to leakage of light to cortical layers along the length of our implanted optic fibers, we tested another group of mice implanted with fibers to deliver light in cortical areas located directly above the dCA1 (*SI Appendix*, Fig. S5*A*). We saw no differences in freezing responses between $ChR2^{VTA/SNc}$ and $YFP^{VTA/SNc}$ (control) mice when we targeted light delivery in cortical areas above dCA1 (*SI Appendix*, Fig. S5*B*). We also did not observe any effect on freezing when we performed the same experiment and delivered light to subcortical areas below the dHip (*SI Appendix*, Fig. S5 *C* and *D*). These data suggest that the enhanced aversive memory (Fig. 3*F*) arose because of DA release in the dCA1.

Finally, we wanted to address the possibility that enhanced DA release in the dCA1 causes generalized fear responses independent of contextual cue associations. To test for generalized fear, we measured freezing in a subgroup of mice 24 h after cFC testing, but this time the animals were placed in a different chamber (altered walls, lighting, scent, and flooring). Neither group exhibited substantial freezing responses to the altered context, and no significant differences were observed between control and ChR2-positive mice (Fig. 3*G*). To test the possibility that the optogenetic stimulation of DA release by itself is responsible for the increase in freezing, we trained mice without foot shock delivery (*SI Appendix*, Fig. S5*E*). When tested the next day, both groups exhibited low freezing, and there were no differences between control and ChR2-positive mice (*SI Appendix*, Fig. S5*F*). These control experiments provide further support that the optogenetic enhancement of DA release from VTA/SNc in the dCA1 facilitates fear acquisition in a strictly context-dependent manner.

Dopaminergic Signaling in dCA1 Is Required for Normal Acquisition of Contextual Fear. To investigate whether dopaminergic signaling in the dCA1 region is required for the acquisition of cFC, we implanted mice with bilateral cannulas over the dCA1 (Fig. 4 *A* and *B*). To block dopaminergic signaling in the dCA1 during cFC acquisition, mice were locally infused with the D1/D5 receptor antagonist, SCH23390 (SCH). Mice were allowed to rest for 15 min after the completion of the infusions before starting the cFC training session. During cFC training, mice explored the conditioning chamber for 2 min, after which they received a series of five mild foot shocks (0.4 mA, 1 s) with pseudorandomized intervals averaging 2 min. The next day, mice returned to the same chamber, and their memory of the aversive context was assessed by measuring the time they spent freezing. Saline-infused control mice displayed robust freezing during the 5 min of testing (Fig. 4*C*, blue bar). Compared to saline, SCH-treated mice displayed significantly decreased freezing (Fig. 4*C*, red bar) during testing. These data indicate that dopaminergic signaling through D1/D5 receptors in the dCA1 is required for the acquisition of contextual fear memories. Furthermore, our results demonstrate that DA regulates aversive learning in the hippocampus bidirectionally. The pharmacological inhibition of DA signaling in dCA1 reduces cFC acquisition, whereas the optogenetic enhancement of DA release from the midbrain facilitates aversive learning.

Normal Formation of Aversive Memory in the Absence of DA Cotransmission from Noradrenergic Terminals in the Dorsal Hippocampus. To test the contribution of DA cotransmission from noradrenergic terminals in the dCA1 to aversive memory formation during cFC, we generated conditional knockout (KO) mice in which TH was specifically ablated from all neurons expressing DA beta-hydroxylase (Dbh), which catalyzes the conversion of DA to NE. Thus, TH is removed from noradrenergic neurons in the LC (TH^{LC} KO), the source of noradrenergic input to the dHip. TH deletion in these neurons is expected to disrupt the biosynthesis of both DA and NE in the LC (Fig. 5*A*). To account for the fetal requirement for NE (41) and rescue lethality, female breeders were treated with adrenergic agonists phenylephrine and isoproterenol (0.1 mg/mL in drinking water) from E8.5 to E16.5 and L-DOPA (4 mg/mL in drinking water) from E16.5 until birth. We examined brain sections from TH^{LC} KO ($Dbh^{Cre/+};Th^{loxP/loxP}$) and heterozygous littermate controls ($Dbh^{Cre/+};Th^{loxP/+}$) after immunostaining against TH to verify the absence of TH in LC noradrenergic neurons. We found that TH immunofluorescence was essentially absent in the LC of TH^{LC} KO mice (Fig. 5 *B* and *C*). As a direct consequence of Dbh-mediated deletion of TH, catecholamine levels were also dramatically reduced in the brainstem of TH^{LC} KO mice compared to littermate controls (Fig. 5 *D* and *E*; note that in some cases DA levels were not zero because of the existence of other [non-Dbh containing] dopaminergic cells in the brainstem). In contrast to the lack of immunofluorescence in the LC, TH levels in the midbrain dopaminergic centers (i.e., VTA and SNc) of TH^{LC} KO mice were indistinguishable from controls (Fig. 5 *F* and *G*). In the dHip, TH immunofluorescence was significantly reduced in the CA1 region of TH^{LC} KO mice (Fig. 6 *A* and *B*), particularly in the SO and SR, while the substantial signal remained in the pyramidal cell area (PCL; Fig. 6*A*). Overall, we observed that approximately one-third of the TH signal in the dCA1 of controls remained in TH^{LC} KO mice. The remaining TH signal in the dCA1 of TH^{LC} KO mice strongly resembled our VTA/SNc innervation to the dCA1 illustrated by the anterograde tracing data (Fig. 1*C*), supporting the notion that it represents midbrain dopaminergic input. Catecholamine content measurements revealed very low levels of NE in the dHip of TH^{LC} KO mice (Fig. 6*C*), while DA showed only a trend toward modest reduction compared to controls (Fig. 6*D*). Taken together, these

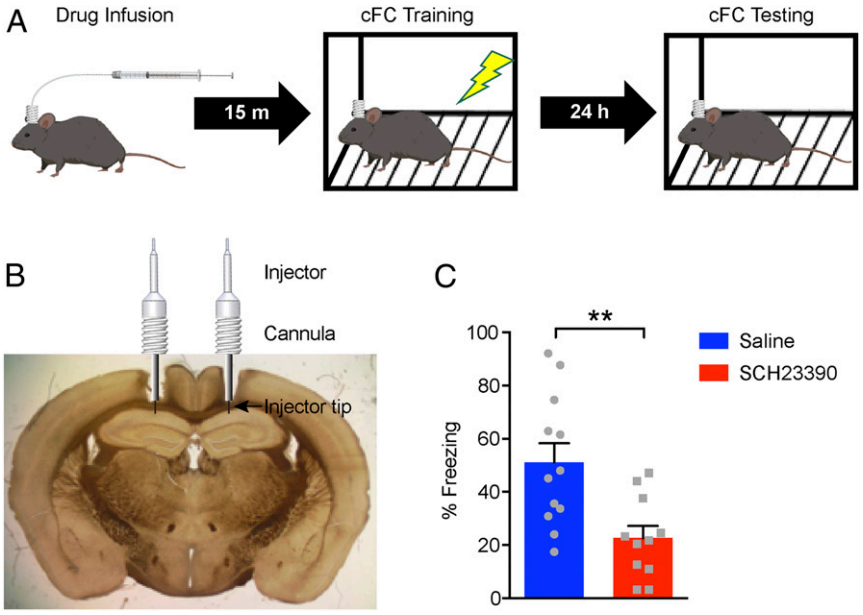

Fig. 4. Inhibition of D1/D5 signaling in hippocampal dCA1 impairs the acquisition of cFC. (*A*) Illustration of the procedure for drug infusions and cFC. Mice were infused with drugs through bilateral cannulas implanted above the hippocampal dCA1. After the completion of infusions, animals were allowed to rest for 15 min and then subjected to cFC training. Around 24 h later, mice were reintroduced to the same chamber to test for freezing. (*B*) Image of a coronal brain slice showing the position of the bilateral cannulas and the graphic illustration of the cannulas and injectors for drug delivery. (*C*) Graph showing the freezing responses of mice treated with vehicle (saline, blue) and SCH (red) to inhibit D1/D5 receptors during cFC testing 24 h later. Unpaired Student's *t* test, $P = 0.0068$; $n = 12$ and 11 for saline and SCH, respectively; $^{**}P < 0.01$; and data represent means ± SEM.

data show that TH^{LC} KO mice exhibit a selective deficit in catecholamine production that is restricted to Dbh-positive neurons.

As a next step, we investigated whether TH^{LC} KO mice would demonstrate any deficits in aversive memory formation during cFC. This allows us to address directly whether DA transmission in the hippocampus from noradrenergic terminals is required for contextual fear learning. To this end, we trained TH^{LC} KO mice and littermate controls with the cFC protocol we used previously (Figs. 3 and 4). When tested 24 h later, both groups showed similar freezing responses (Fig. 6*E*). To corroborate these findings, we tested a second experimental animal cohort under entirely different experimental parameters. Specifically, mice were trained and tested in another laboratory, utilizing different equipment and experimental conditions (different light/dark cycle, shock number, and intensity—for details refer to the *Materials and Methods*). Again, the fear responses of TH^{LC} KO mice were indistinguishable from controls when tested 1 d after cFC training (Fig. 6*F*). These results demonstrate that mice can perform the cFC task even in the absence of NE or concomitant DA release from noradrenergic terminals in the hippocampus, suggesting that midbrain DA transmission is sufficient to support normal aversive learning.

Discussion

Topology of Midbrain Dopaminergic Innervation of the Dorsal Hippocampus. Although midbrain DA neurons have been classically considered to be inhibited by aversive stimuli (42, 43), recent studies have identified dopaminergic subpopulations that are excited by aversive or noxious stimuli (28, 34, 44, 45). Most of the research that was done to identify the circuitry that mediates such responses has focused on the mesolimbic DA system, which includes VTA DA neurons projecting to the nucleus accumbens (33, 46). Based on these data, glutamatergic inputs from the lateral habenula, a region that is excited by aversive stimuli (47), activate a subpopulation of VTA DA neurons that sends projections to the ventral nucleus accumbens (NAc) medial shell in response to conditioned aversive stimuli (33). Interestingly, DA terminals in all other NAc regions are inhibited by the same aversive signals (33). Thus, the cell-type and region-specific afferent control of subpopulations of a highly diverse midbrain dopaminergic system dictates DA neuron responses to aversive stimuli.

Despite the evidence for a role of DA signaling in the hippocampus, there is very limited information on the location of midbrain DA neurons that send afferents to the hippocampal formation. In fact, several large-scale input–output tracing efforts (11, 12, 48) have omitted the hippocampus from their analysis, mainly because of the sparse dopaminergic innervation in this area. Older retrograde and anterograde studies in the rat did identify projections from the VTA/SNc to the hippocampus (13–15), and recent viral anterograde tracing has labeled TH-positive terminals in the dCA1 originating from VTA/SNc (10, 36). Nonetheless, until now, there was no concrete information about the precise location of a DA neuronal population that sends direct projections to the hippocampus.

In this study, we utilized two viral retrograde strategies based on CAV2 to identify and label midbrain DA neurons that innervate the hippocampus (Fig. 2). Both methods produced similar results, labeling a population of DA neurons near the interface of SNc and lateral VTA (Fig. 2 *C* and *F*) ∼3 mm posterior to bregma. VTA/SNc projections to the hippocampus that we detected appeared to be unilateral; no noticeable labeling was observed on the contralateral side. However, because of the very low efficiency of retrograde transport for CAV2 particles, we cannot exclude the possibility of a lower extent of innervation from the contralateral VTA/SNc to the hippocampus. Ex vivo electrophysiological recordings showed that these cells had I_h currents and that their basal properties were similar to neighboring DA neurons (*SI Appendix*, Fig. S2). These data add important information to the topographical chart of VTA/SNc connectivity, with a focus on a target region like the hippocampus that has often been overlooked in DA circuit-mapping analyses.

A few recent studies, including ours, have attempted to map midbrain dopaminergic projections to the hippocampal field using axon-targeted ChR2 viral methodologies (18, 24, 25). All of these studies have provided similar results that showed sparse

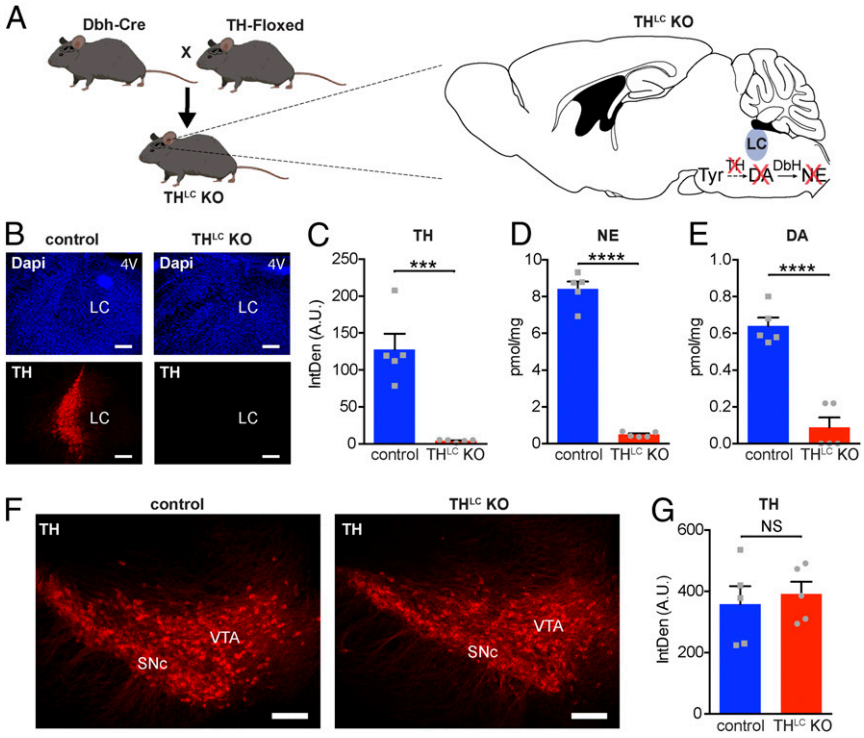

Fig. 5. Generation and characterization of LC TH-deficient mice (TH^{LC} KO). (*A*) A simplified graphical illustration of the breeding for the generation of TH^{LC} KO mice, resulting in the genetic ablation of DA and NE production in the LC (see *Materials and Methods* section for the detailed breeding information). (*B*) Coronal sections of the LC of TH^{LC} KO and a littermate control stained for DAPI (blue, *Top*) and TH (red, *Bottom*). 4V represents the fourth ventricle. (Scale bars, 200 μm.) (*C*) Bar graphs showing the integrated density (IntDen) of TH immunofluorescence in the LC of control and TH^{LC} KO mice. Unpaired Student's *t* test, $P = 0.0004$; $n = 5$ for control and TH^{LC} KO; ***$P < 0.001$; and data represent means ± SEM. (*D*) Bar graphs showing the tissue content of NE in the brainstem of control and TH^{LC} KO mice. Unpaired Student's *t* test, $P < 0.0001$; $n = 5$ for control and TH^{LC} KO; ****$P < 0.0001$; and data represent means ± SEM. (*E*) Bar graphs showing the tissue content of DA in the brainstem of control and TH^{LC} KO mice. Unpaired Student's *t* test, $P < 0.0001$; $n = 5$ for control and TH^{LC} KO; ****$P < 0.0001$; and data represent means ± SEM. (*F*) Coronal midbrain sections of TH^{LC} KO and a littermate control stained for TH (red). (Scale bars, 100 μm.) (*G*) Bar graphs showing the IntDen of TH immunofluorescence in the midbrain of control and TH^{LC} KO mice. Unpaired Student's *t* test, $P = 0.6545$; $n = 5$ for control and TH^{LC} KO; not significant (NS): $P > 0.05$; and data represent means ± SEM. A.U., arbitrary units.

innervation with only a limited number of dopaminergic fibers present in the dHip and the dCA1 region in particular. Since ChR2 is not an anterograde tracer, it is likely that these results underestimated the amount of hippocampal innervation that stems from midbrain dopaminergic sources. Therefore, we took advantage of an anterograde viral approach that provides a very concentrated fluorescence signal in axonal terminals to label midbrain dopaminergic projections in dCA1. The midbrain innervation of the hippocampus was verified by the anterograde labeling of DA terminals with a synaptophysin-mRuby fusion protein (Fig. 1). This approach boosts the fluorescent signal because synaptophysin is multiply expressed in the many synaptic vesicles of the terminals. Using this technique, we uncovered additional DA input to the dCA1 field covering the entire PCL, a signal we and others did not observe with ChR2-related approaches (Fig. 3*C*). We verified that this signal was indeed dopaminergic, as it colocalized perfectly with TH (Fig. 1 *D*–*F*). Our observations found additional support when we genetically ablated TH production in noradrenergic neurons, eliminating the TH signal coming to the hippocampus from the LC. The remaining TH labeling originating from the midbrain included sparse TH-positive fibers in the SO and SR, which were more dense but similar to what we saw when we labeled DA fibers with ChR2 (Fig. 3*C*). However, the majority of the remaining TH signal spanned the PCL in dCA1, in a similar fashion to the signal we observed using our anterograde, viral labeling of the TH-positive terminals (Fig. 1). Other approaches have failed to unveil this innervation, creating the misconception that DA functionality comes almost entirely from alternative sources, such as the LC. Although this may be correct for some kinds of spatial memory retention, our data show that DA originating from VTA/SNc is sufficient to support normal aversive memory formation in the dHip during cFC (Fig. 6 *E* and *F*).

Dopaminergic Modulation of Aversive Memory Encoding during cFC. The effective recall of negative experiences is important for survival because it can help organisms avoid threatening situations they have confronted in the past. The encoding of aversive memories relies heavily on the formation of an association between the negative experience and the spatial setting where the experience has occurred. This process is referred to as context conditioning, and it has been shown to depend strongly on hippocampal function (49, 50), especially the dCA1 (51). Studies utilizing inhibitory avoidance as a paradigm to assess aversive memory have demonstrated the importance of dopaminergic signaling in the dHip for the persistence of aversive learning (10, 35, 52). The inhibition of DA transmission via the local administration of a D1-like receptor antagonist in dCA1 shortly before training resulted in memory impairment (10), while the same treatment immediately after training had no effect (10, 35), supporting a modulatory role for DA during encoding of aversive learning.

We showed that the inhibition of D1/D5 receptors in the dCA1 during cFC training impairs memory recall 24 h later (Fig. 4). Moreover, we demonstrated that the optogenetic activation of release from midbrain dopaminergic terminals in dCA1 during the acquisition of cFC results in increased fear responses

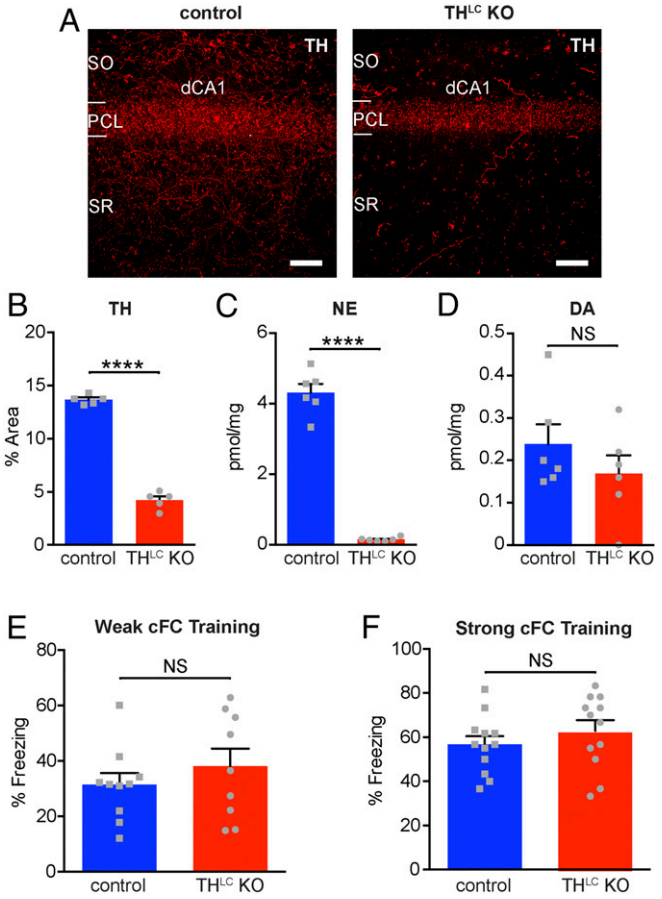

Fig. 6. Genetic ablation of catecholamine production in the LC does not affect normal aversive learning. (*A*) Coronal sections of the dCA1 hippocampal region from a TH^{LC} KO and a littermate control stained for TH (red). (Scale bars, 50 μm.) (*B*) Bar graphs showing the percent of the total pixel area containing TH immunofluorescence in the dCA1 of control and TH^{LC} KO mice. Unpaired Student's *t* test, $P < 0.0001$; $n = 5$ for control and TH^{LC} KO; ****$P < 0.0001$; and data represent means ± SEM. (*C*) Bar graphs showing the tissue content of NE in the dHip of control and TH^{LC} KO mice. Unpaired Student's *t* test, $P < 0.0001$; $n = 6$ for control and TH^{LC} KO; ***$P < 0.0001$; and data represent means ± SEM. (*D*) Bar graphs showing the tissue content of DA in the dHip of control and TH^{LC} KO mice. Unpaired Student's *t* test, $P = 0.3002$; $n = 6$ for control and TH^{LC} KO; not significant (NS): $P > 0.05$; and data represent means ± SEM. (*E*) Graph showing the freezing responses of TH^{LC} KO and control mice after reexposure to the same context 24 h after training with a weak cFC protocol. Unpaired Student's *t* test, $P = 0.3839$; $n = 10$ and 9 for control and TH^{LC} KO, respectively; NS: $P > 0.05$; and data represent means ± SEM. (*F*) Graph showing the freezing responses of TH^{LC} KO and control mice after reexposure to the same context 24 h after strong cFC training. Unpaired Student's *t* test, $P = 0.3175$; $n = 12$ for control and TH^{LC} KO; NS: $P > 0.05$; and data represent means ± SEM.

during recall 1 d later (Fig. 3). This effect was context dependent (Fig. 3*G*) and was not due to generalized fear. These data indicate that increased hippocampal DA enhances aversive learning during the encoding phase to establish a long-term fear memory. Additionally, our results support the idea that DA is important for the formation of an association between the spatial context and the aversive stimulus, and the additional activation of DA release from terminals originating from the VTA/SNc can make this association stronger.

Several lines of evidence indicate that midbrain dopaminergic innervation can modulate synaptic plasticity in the hippocampus, a phenomenon that contributes to memory retention. Midbrain DA signaling is important during nicotine-induced synaptic plasticity in the hippocampus (17) and for the Schaffer collateral synaptic plasticity associated with an inhibitory avoidance task (10). The optogenetic activation of hippocampal DA fibers originating from the VTA in mice exploring a context increased hippocampal reactivation (18) and enhanced spatial learning and memory (18, 25). More specifically, DA transmission within the dCA1 has been shown to regulate the late phase of long-term potentiation (LTP) of Schaffer collateral synapses (53–55). This process requires protein synthesis and is believed to be the underlying mechanism of hippocampal memory consolidation (56, 57). Additionally, DA signaling was shown to facilitate LTP induction when weak and subthreshold induction protocols were used both in vivo (58) and in hippocampal slices (59). Interestingly, it was also demonstrated that DA can extend the time window for successful spike timing-dependent plasticity in the hippocampus (60, 61). Although most of these studies were performed using bath-applied DA or DA receptor agonists/antagonists, a later study in hippocampal slices (16) demonstrated that the optogenetic stimulation of dopaminergic terminals originating from the VTA/SNc, with a protocol that simulates phasic firing, causes the potentiation of excitatory synaptic transmission of Schaffer collateral synapses.

In our experiments, we coupled the phasic optogenetic stimulation of DA release with foot shock delivery during the acquisition phase of cFC. This resulted in the formation of a stronger fear memory, as mice exhibited higher-freezing responses during recall (Fig. 3). Interestingly, when DA stimulation was performed after training, and it was not coupled with the aversive foot-shocks, no differences in freezing were observed (*SI Appendix*, Fig. S4*D*). These results could also be explained through the synaptic tagging and capture hypothesis (8, 62). According to this theory, DA neurotransmission in the dCA1 facilitates the association of the spatial context with the aversive foot shock. This association arises via an increase in plasticity-related proteins that induce experience-dependent synaptic changes and thereby promote long-term aversive memory formation. Overall, DA signaling during an aversive, contextual task could serve as a functional label of threatening cues by enabling and modulating hippocampal synaptic mechanisms that underlie learning.

There are still many open questions regarding the midbrain DA regulation of aversive learning in the dHip. What are the cellular and physiological substrates of DA action to enhance aversive learning performance? Could the differences in learning be compensated by extended training or would they persist? Moreover, could aversive memories be overwritten by optogenetically stimulating DA in dCA1 in the same context without foot shock the day after training? Additional research on the timing and the effects of DA stimulation in the dCA1 would provide important insights into the regulation of aversive learning.

Materials and Methods

Mice. C57BL/6J, DAT-Cre, and Ai14 mice were purchased from the Jackson Laboratory. Adult male mice (3 to 6 mo old) were used for behavioral experiments, and both male and female mice (8 to 12 wk old) were used for immunohistochemistry and anatomical tracing. Mice were housed on a 12-h light/dark cycle (lights on at 21:00) with rodent chow and water ad libitum. All behavioral procedures were performed during the dark cycle (i.e., awake period), except for the experiment in Fig. 6*F*, which was performed during the light cycle of the mice. Prior to testing, mice were acclimated to the test room for at least 30 min. All experiments complied with the animal care standards of the NIH and were approved by the Institutional Animal Care and Use Committee of the University of Pennsylvania.

Stereotactic Surgeries. All stereotactic procedures were performed using a stereotaxic instrument under inhaled isoflurane anesthesia (Angle Two, Leica Biosystems). The animal's body temperature was kept stable by using a feedback-controlled heating pad during surgery and during recovery from anesthesia. For optogenetics experiments, 0.5 to 1 μL concentrated AAV solution (AAV5-EF1a–DIO-hChR2[H134R]-eYFP; AAV5-EF1a-DIO-eYFP; ~10^{12} infectious units per milliliter, prepared by the University of North Carolina

Vector Core Facility) was injected bilaterally into the lateral VTA/SNc (bregma: −3.25 mm, lateral: ±0.50 mm, and ventral: −4.40 mm) at a rate of 200 nL/min using a syringe pump (KD Scientific). The injection needle was left at the injection site for 10 min after the end of the infusion before being withdrawn. After the completion of viral injections, mice received the bilateral implantation of chronic optical fibers (200-μm diameter; numerical aperture = 0.50; Thorlabs) dorsal to the hippocampal CA1 (dCA1; bregma: −1.45 mm, lateral: ±1.00 mm, ventral: −1.05 mm, and angle: ±5°). For pharmacological experiments, a bilateral guide cannula (26 gauge, 3 mm long; 2 mm center to center; Plastics One) was chronically implanted in the same CA1 region and secured to the skull with adhesive cement (C&B Metabond; Parkell). For retrograde tracing and labeling, 1 μL CAV solution (CAV2-Cre; CAV2-Flex-Flpo; $\sim 5 \times 10^{12}$ physical particles per milliliter, prepared by the Vector Platform of the University of Montpellier) was injected into the dHip (bregma: −1.80 mm, lateral: 1.00 mm, and ventral: −1.50 mm). Experiments were performed 8 to 12 wk (for AAVs) or 3 to 5 d (for CAV-2) after stereotactic injection. Coronal sections (50 to 70 μm in thickness) were prepared from all injected and implanted mice to verify the proper location of injection sites and optical fiber and cannula placements.

cFC. cFC was performed in a sound-vaulted, red-lit room during the dark cycle of the mice. The mice were acclimated to the room for 30 min before fear conditioning training and testing. For the training day, the grid floor of the fear-conditioning chamber was connected to a shock generator (Coulbourn). Prior to each mouse being placed into the chamber, the chamber was cleaned with 20% ethanol solution. The protocol was set to allow the mouse 2 min to become acclimated to the chamber followed by a 9-min period over which five foot shocks (0.4 mA, 1 s) were delivered in pseudorandomized intervals averaging 2 min. The mouse remained in the chamber for an additional minute after the delivery of the last foot shock before returning to its home cage. For optogenetic manipulations, blue light was generated by a 450-nm laser (Changchun New Industries) and delivered at 10 mW power (measured at the tip of the optic fibers) to stimulate fibers in the dCA1. Each mouse was connected to the laser via bilateral optic fiber cables (Doric Lenses) coupled to their implanted optic fiber cannulas. A pulse generator was coupled to the laser and was activated by a transistor–transistor logic (TTL) signal originating from the fear conditioning software (FreezeFrame, Actimetrics). This TTL signal was delivered together with the first foot shock and triggered blue-light pulses (10 ms at 20 Hz for 1 s every 10 s) that continued until the end of the protocol. Testing occurred ∼24 h after training, with all the mice returning to the same fear-conditioning chamber for a total period of 5 min. Mice that received light stimulation during training were again connected with optic fiber cables, but this time no light was delivered. Fear-conditioning testing in a different context occurred 24 h later. Mice were placed for 2 min in a different chamber (floor and walls were changed, and vanilla scent was sprayed in the chamber) with no optic fiber cables attached. For every session, the mouse behavior was recorded, and the amount of time the mouse spent freezing (immobility bouts greater than 1 s) was calculated using the FreezeFrame software. Freezing was scored by an individual who was unaware of the experimental conditions, animal genotypes, or treatments. For the experimental results illustrated in Fig. 6*F*, a different training protocol was used to verify that our results were not protocol dependent. Animals were placed in the training apparatus (ENV-010MC with ENV-414S, Med Associates) for 2 min, after which a single 2 s, 1 mA foot shock was delivered. The animals were removed from the apparatus 30 s later and returned to their home cages. The apparatus was cleaned with Versa-Clean (Thermo Fisher Scientific) between subjects.

Histology, Immunofluorescence, and Imaging. Histological processing, immunofluorescence staining, and microscopy were performed as described previously (63, 64). Following intracardial perfusion with 4% paraformaldehyde in phosphate-buffered saline, pH 7.4, mouse brains were removed and postfixed overnight. Coronal sections (50 to 70 μm) from the hippocampus, midbrain, and LC were prepared in a vibratome (Leica). Sections were stained overnight with primary antibodies against TH (rabbit anti-TH, 1:500, Millipore) and GFP (mouse anti-GFP, 1:1,000, Thermo Fisher Scientific). The next day, sections were stained with compatible Alexa Fluor goat secondary antibodies (1:250, Thermo Fisher Scientific) for 2 h. For high-resolution images, acquisition was performed with a Leica SP5 laser-scanning confocal microscope using 40× or 60× objectives. For lower resolution, images were taken using 5× and 10× objectives of an Olympus BX63 automated fluorescence microscope. Images were analyzed using ImageJ, and quantifications were performed by averaging values from 6 to 10 sections per animal after applying similar thresholding parameters among all images. Sections were labeled relative to bregma according to "The Mouse Brain in Stereotaxic Coordinates" (65).

Statistical Analysis. Statistical analyses were performed with Prism (GraphPad) software. For comparisons between two groups, two-tailed unpaired *t* tests were used, whereas differences across more than two groups were analyzed with one-way or two-way ANOVA, followed by Dunnett's post hoc test to account for multiple comparisons. All experimental data are reported as mean ± SEM. Differences where $P < 0.05$ are considered statistically significant.

Data Availability. Mouse lines will be available upon request from the corresponding authors. All other study data are included in the article and/or supporting information.

ACKNOWLEDGMENTS. We thank Marion Scott and Elizabeth Menne for excellent technical assistance and Tiffany Brown-Mangum and Tyisha Hundley for help with animal husbandry. We are grateful to Karl Deisseroth and Charu Ramakrishnan for AAV vectors and to Richard Palmiter for providing the floxed *Th* mice. We also thank Marc Fuccillo and Alexey Ostroumov for helpful discussions and insightful feedback on the manuscript draft. Targeted embryonic stem cell injections were performed by the Transgenic and Chimeric Mouse Facility at the University of Pennsylvania. This work was supported by grants from the NIH (NS021229 and AA026267 to J.A.D. and MH080333 to S.A.T.) and NIH/*Eunice Kennedy Shriver* National Institute of Child Health and Human Development U54 Grant HD086984 to the Institutional Intellectual and Developmental Disabilities Research Center of the Children's Hospital of Philadelphia and University of Pennsylvania. This work was also supported by a generous award from the Chernowitz Medical Research Foundation.

1. W. Schultz, Multiple dopamine functions at different time courses. *Annu. Rev. Neurosci.* **30**, 259–288 (2007).
2. A. M. Graybiel, T. Aosaki, A. W. Flaherty, M. Kimura, The basal ganglia and adaptive motor control. *Science* **265**, 1826–1831 (1994).
3. A. V. Kravitz *et al*., Regulation of parkinsonian motor behaviours by optogenetic control of basal ganglia circuitry. *Nature* **466**, 622–626 (2010).
4. M. Matsumoto, O. Hikosaka, Two types of dopamine neuron distinctly convey positive and negative motivational signals. *Nature* **459**, 837–841 (2009).
5. B. T. Saunders, J. M. Richard, E. B. Margolis, P. H. Janak, Dopamine neurons create Pavlovian conditioned stimuli with circuit-defined motivational properties. *Nat. Neurosci.* **21**, 1072–1083 (2018).
6. W. Schultz, P. Apicella, T. Ljungberg, Responses of monkey dopamine neurons to reward and conditioned stimuli during successive steps of learning a delayed response task. *J. Neurosci.* **13**, 900–913 (1993).
7. N. S. Bamford, R. M. Wightman, D. Sulzer, Dopamine's effects on corticostriatal synapses during reward-based behaviors. *Neuron* **97**, 494–510 (2018).
8. J. Lisman, A. A. Grace, E. Duzel, A neoHebbian framework for episodic memory; role of dopamine-dependent late LTP. *Trends Neurosci.* **34**, 536–547 (2011).
9. J. E. Lisman, A. A. Grace, The hippocampal-VTA loop: Controlling the entry of information into long-term memory. *Neuron* **46**, 703–713 (2005).
10. J. I. Broussard *et al*., Dopamine regulates aversive contextual learning and associated in vivo synaptic plasticity in the hippocampus. *Cell Rep.* **14**, 1930–1939 (2016).
11. K. T. Beier *et al*., Circuit architecture of VTA dopamine neurons revealed by systematic input-output mapping. *Cell* **162**, 622–634 (2015).
12. J.-F. Poulin *et al*., Mapping projections of molecularly defined dopamine neuron subtypes using intersectional genetic approaches. *Nat. Neurosci.* **21**, 1260–1271 (2018).
13. A. Gasbarri, M. G. Packard, E. Campana, C. Pacitti, Anterograde and retrograde tracing of projections from the ventral tegmental area to the hippocampal formation in the rat. *Brain Res. Bull.* **33**, 445–452 (1994).
14. A. Gasbarri, C. Verney, R. Innocenzi, E. Campana, C. Pacitti, Mesolimbic dopaminergic neurons innervating the hippocampal formation in the rat: A combined retrograde tracing and immunohistochemical study. *Brain Res.* **668**, 71–79 (1994).
15. A. Gasbarri, A. Sulli, M. G. Packard, The dopaminergic mesencephalic projections to the hippocampal formation in the rat. *Prog. Neuropsychopharmacol. Biol. Psychiatry* **21**, 1–22 (1997).
16. Z. B. Rosen, S. Cheung, S. A. Siegelbaum, Midbrain dopamine neurons bidirectionally regulate CA3-CA1 synaptic drive. *Nat. Neurosci.* **18**, 1763–1771 (2015).
17. J. Tang, J. A. Dani, Dopamine enables in vivo synaptic plasticity associated with the addictive drug nicotine. *Neuron* **63**, 673–682 (2009).
18. C. G. McNamara, Á. Tejero-Cantero, S. Trouche, N. Campo-Urriza, D. Dupret, Dopaminergic neurons promote hippocampal reactivation and spatial memory persistence. *Nat. Neurosci.* **17**, 1658–1660 (2014).
19. J. Sariñana, T. Kitamura, P. Künzler, L. Sultzman, S. Tonegawa, Differential roles of the dopamine 1-class receptors, D1R and D5R, in hippocampal dependent memory. *Proc. Natl. Acad. Sci. U.S.A.* **111**, 8245–8250 (2014).
20. E. Puighermanal *et al*., Anatomical and molecular characterization of dopamine D1 receptor-expressing neurons of the mouse CA1 dorsal hippocampus. *Brain Struct. Funct.* **222**, 1897–1911 (2017).

21. Y. Mu, C. Zhao, F. H. Gage, Dopaminergic modulation of cortical inputs during maturation of adult-born dentate granule cells. *J. Neurosci.* **31**, 4113–4123 (2011).
22. C. C. Smith, R. W. Greene, CNS dopamine transmission mediated by noradrenergic innervation. *J. Neurosci.* **32**, 6072–6080 (2012).
23. P. Devoto, G. Flore, L. Pani, G. L. Gessa, Evidence for co-release of noradrenaline and dopamine from noradrenergic neurons in the cerebral cortex. *Mol. Psychiatry* **6**, 657–664 (2001).
24. T. Takeuchi *et al*., Locus coeruleus and dopaminergic consolidation of everyday memory. *Nature* **537**, 357–362 (2016).
25. K. A. Kempadoo, E. V. Mosharov, S. J. Choi, D. Sulzer, E. R. Kandel, Dopamine release from the locus coeruleus to the dorsal hippocampus promotes spatial learning and memory. *Proc. Natl. Acad. Sci. U.S.A.* **113**, 14835–14840 (2016).
26. N. Lemon, S. Aydin-Abidin, K. Funke, D. Manahan-Vaughan, Locus coeruleus activation facilitates memory encoding and induces hippocampal LTD that depends on β-adrenergic receptor activation. *Cereb. Cortex* **19**, 2827–2837 (2009).
27. S. J. Sara, The locus coeruleus and noradrenergic modulation of cognition. *Nat. Rev. Neurosci.* **10**, 211–223 (2009).
28. F. Brischoux, S. Chakraborty, D. I. Brierley, M. A. Ungless, Phasic excitation of dopamine neurons in ventral VTA by noxious stimuli. *Proc. Natl. Acad. Sci. U.S.A.* **106**, 4894–4899 (2009).
29. D. V. Wang, J. Z. Tsien, Convergent processing of both positive and negative motivational signals by the VTA dopamine neuronal populations. *PLoS One* **6**, e17047 (2011).
30. B. B. Gore, M. E. Soden, L. S. Zweifel, Visualization of plasticity in fear-evoked calcium signals in midbrain dopamine neurons. *Learn. Mem.* **21**, 575–579 (2014).
31. F. A. Guarraci, B. S. Kapp, An electrophysiological characterization of ventral tegmental area dopaminergic neurons during differential pavlovian fear conditioning in the awake rabbit. *Behav. Brain Res.* **99**, 169–179 (1999).
32. E. A. Budygin *et al*., Aversive stimulus differentially triggers subsecond dopamine release in reward regions. *Neuroscience* **201**, 331–337 (2012).
33. J. W. de Jong *et al*., A neural circuit mechanism for encoding aversive stimuli in the mesolimbic dopamine system. *Neuron* **101**, 133–151.e7. (2019).
34. S. Lammel, D. I. Ion, J. Roeper, R. C. Malenka, Projection-specific modulation of dopamine neuron synapses by aversive and rewarding stimuli. *Neuron* **70**, 855–862 (2011).
35. J. I. Rossato, L. R. M. Bevilaqua, I. Izquierdo, J. H. Medina, M. Cammarota, Dopamine controls persistence of long-term memory storage. *Science* **325**, 1017–1020 (2009).
36. L. Faget *et al*., Opponent control of behavioral reinforcement by inhibitory and excitatory projections from the ventral pallidum. *Nat. Commun.* **9**, 849 (2018).
37. C. Soudais, C. Laplace-Builhe, K. Kissa, E. J. Kremer, Preferential transduction of neurons by canine adenovirus vectors and their efficient retrograde transport in vivo. *FASEB J.* **15**, 2283–2285 (2001).
38. L. Madisen *et al*., A robust and high-throughput Cre reporting and characterization system for the whole mouse brain. *Nat. Neurosci.* **13**, 133–140 (2010).
39. M. S. Fanselow, A. M. Poulos, The neuroscience of mammalian associative learning. *Annu. Rev. Psychol.* **56**, 207–234 (2005).
40. S. Lammel *et al*., Diversity of transgenic mouse models for selective targeting of midbrain dopamine neurons. *Neuron* **85**, 429–438 (2015).
41. S. A. Thomas, A. M. Matsumoto, R. D. Palmiter, Noradrenaline is essential for mouse fetal development. *Nature* **374**, 643–646 (1995).
42. J. Mirenowicz, W. Schultz, Preferential activation of midbrain dopamine neurons by appetitive rather than aversive stimuli. *Nature* **379**, 449–451 (1996).
43. M. A. Ungless, P. J. Magill, J. P. Bolam, Uniform inhibition of dopamine neurons in the ventral tegmental area by aversive stimuli. *Science* **303**, 2040–2042 (2004).
44. S. Lammel, B. K. Lim, R. C. Malenka, Reward and aversion in a heterogeneous midbrain dopamine system. *Neuropharmacology* **76**, 351–359 (2014).
45. S. Lammel *et al*., Input-specific control of reward and aversion in the ventral tegmental area. *Nature* **491**, 212–217 (2012).
46. A. M. Brooks, G. S. Berns, Aversive stimuli and loss in the mesocorticolimbic dopamine system. *Trends Cogn. Sci.* **17**, 281–286 (2013).
47. M. Matsumoto, O. Hikosaka, Lateral habenula as a source of negative reward signals in dopamine neurons. *Nature* **447**, 1111–1115 (2007).
48. T. N. Lerner *et al*., Intact-brain analyses reveal distinct information carried by SNc dopamine subcircuits. *Cell* **162**, 635–647 (2015).
49. J. J. Kim, M. S. Fanselow, Modality-specific retrograde amnesia of fear. *Science* **256**, 675–677 (1992).
50. S. Maren, G. Aharonov, M. S. Fanselow, Neurotoxic lesions of the dorsal hippocampus and Pavlovian fear conditioning in rats. *Behav. Brain Res.* **88**, 261–274 (1997).
51. I. Goshen *et al*., Dynamics of retrieval strategies for remote memories. *Cell* **147**, 678–689 (2011).
52. D. Moncada, F. Ballarini, M. C. Martinez, J. U. Frey, H. Viola, Identification of transmitter systems and learning tag molecules involved in behavioral tagging during memory formation. *Proc. Natl. Acad. Sci. U.S.A.* **108**, 12931–12936 (2011).
53. U. Frey, H. Matthies, K. G. Reymann, H. Matthies, The effect of dopaminergic D1 receptor blockade during tetanization on the expression of long-term potentiation in the rat CA1 region in vitro. *Neurosci. Lett.* **129**, 111–114 (1991).
54. Y. Y. Huang, E. R. Kandel, D1/D5 receptor agonists induce a protein synthesis-dependent late potentiation in the CA1 region of the hippocampus. *Proc. Natl. Acad. Sci. U.S.A.* **92**, 2446–2450 (1995).
55. N. Hansen, D. Manahan-Vaughan, Dopamine D1/D5 receptors mediate informational saliency that promotes persistent hippocampal long-term plasticity. *Cereb. Cortex* **24**, 845–858 (2014).
56. R. C. Malenka, R. A. Nicoll, Long-term potentiation—A decade of progress? *Science* **285**, 1870–1874 (1999).
57. J. P. Johansen, C. K. Cain, L. E. Ostroff, J. E. LeDoux, Molecular mechanisms of fear learning and memory. *Cell* **147**, 509–524 (2011).
58. S. Li, W. K. Cullen, R. Anwyl, M. J. Rowan, Dopamine-dependent facilitation of LTP induction in hippocampal CA1 by exposure to spatial novelty. *Nat. Neurosci.* **6**, 526–531 (2003).
59. J. Swant, J. J. Wagner, Dopamine transporter blockade increases LTP in the CA1 region of the rat hippocampus via activation of the D3 dopamine receptor. *Learn. Mem.* **13**, 161–167 (2006).
60. K. Yang, J. A. Dani, Dopamine D1 and D5 receptors modulate spike timing-dependent plasticity at medial perforant path to dentate granule cell synapses. *J. Neurosci.* **34**, 15888–15897 (2014).
61. E. Edelmann, V. Lessmann, Dopamine modulates spike timing-dependent plasticity and action potential properties in CA1 pyramidal neurons of acute rat hippocampal slices. *Front. Synaptic Neurosci.* **3**, 6 (2011).
62. U. Frey, R. G. Morris, Synaptic tagging and long-term potentiation. *Nature* **385**, 533–536 (1997).
63. T. Tsetsenis *et al*., Rab3B protein is required for long-term depression of hippocampal inhibitory synapses and for normal reversal learning. *Proc. Natl. Acad. Sci. U.S.A.* **108**, 14300–14305 (2011).
64. T. Tsetsenis, A. A. Boucard, D. Araç, A. T. Brunger, T. C. Südhof, Direct visualization of trans-synaptic neurexin-neuroligin interactions during synapse formation. *J. Neurosci.* **34**, 15083–15096 (2014).
65. K. B. J. Franklin, G. Paxinos, *The Mouse Brain in Stereotaxic Coordinates* (Academic Press, ed. 3, 2008).